

# Coherent $\omega$ photoproduction from nuclei and $\omega$ properties in nuclear matter.

A. Sibirtsev<sup>1</sup>, Ch. Elster<sup>1,2</sup> and J. Speth<sup>1</sup>

<sup>1</sup> Institut für Kernphysik, Forschungszentrum Jülich, D-52425 Jülich

<sup>2</sup> Institute of Nuclear and Particle Physics, Ohio University, Athens, OH 45701

Received: date / Revised version: date

**Abstract.** The coherent  $\omega$ -meson photoproduction from nuclei is proposed as a phenomenological method to evaluate the momentum dependence of  $\omega$ -meson mass shift and width in nuclear matter. We analyze available data on un-separated coherent and incoherent  $\omega$ -meson photoproduction from nuclei and extract the imaginary part of the the complex forward  $\omega N$  scattering amplitude, which is proportional to the in-medium  $\omega$ -meson width. The accuracy of the currently available data is not sufficient to evaluate the real part of forward  $\omega N$  scattering amplitude and reconstruct the momentum dependence of the mass shift of the  $\omega$ -meson.

**PACS.** 11.80.La Multiple scattering – 13.60.Le Meson production – 24.10.Ht Diffraction models – 25.20.Lj Photoproduction reactions

## 1 Introduction

The properties of  $\rho$  and  $\omega$  mesons in a nuclear medium remain a topic of extreme interest since the first experimental observations by the CERES and HELIOS-3 Collaborations report of a strong enhancement of low mass dilepton production from heavy ion collisions [1, 2, 3, 4]. This enhancement was interpreted as a modification of the mass and width of the  $\rho$  and  $\omega$  mesons in dense hadronic matter [5, 6, 7, 8]. The  $\rho$ -meson is quite broad in the vacuum and an additional increase of its width in the hadronic environment leads to the production of an almost continuum dilepton spectrum, which does not indicate a resonance structure and can be identified as perpetual spectral strength of the isovector current.

While the  $\rho$ -meson seems to be absolutely melted in matter, one expects that the signal of the  $\omega$ -meson might survive as a quasi resonance structure, even if being strongly modified. More dedicated experiments aim to isolate the  $\omega$ -meson produced in the nuclear medium either by high resolution dilepton spectroscopy [9, 10, 11, 12, 13] or through the  $\omega \rightarrow \pi^0 \gamma$  decay mode [14, 15]. The goal of these experiments is to identify the structure of the  $\omega$ -meson and to measure its width and pole position.

The experimental studies of the in-medium modification of the  $\omega$ -meson mass and width are planned by utilizing pion, proton and heavy ion beams with HADES at GSI [9, 10, 11, 16, 17], with photo-nuclear reactions [14, 18] at TAPS [19] and Crystal Barrel [20] at ELSA, by heavy ion collisions with PHENIX at RHIC [12, 13] and with proton-nucleus reactions by ANKE at COSY [15, 21].

Very recently the E325 experiment at KEK-PS reported [29] new results on the  $\rho/\omega$  meson modification in nuclear matter. It was found that the dielectron spectra produced in  $p+C$  and  $p+Cu$  collisions at proton beam energy of 12 GeV indicate a significant difference below the  $\omega$ -meson mass. The enhancement of the invariant mass spectra of electron-positron pairs produced from a heavy  $Cu$  target might suggest the modification of the  $\rho/\omega$  properties at normal nuclear density and for average  $\omega$ -meson momenta  $k_\omega \simeq 1$  GeV.

Obviously, apart of the heavy ion reactions, in the above mentioned experiments the  $\omega$ -mesons are produced with a certain laboratory momenta  $k_\omega$ , that can be quite large. The scale of  $k_\omega$  is defined by the threshold of the relevant elementary  $\omega$ -meson production reaction. On the other hand, currently available predictions [22, 23, 24, 25, 26, 27] for the in-medium modification of the  $\omega$ -meson mass and width are given for the  $\omega$ -meson at rest, i.e. for momentum  $k_\omega=0$ .

Only some estimates are presently available [23, 24, 28] for finite  $k_\omega$  and they are model dependent. These predictions [23, 24, 28] are obtained by calculations of a forward  $\omega N$  scattering amplitude  $f_{\omega N}$ , which within the low density approximation is related to an additional in-medium collisional  $\omega$ -meson width  $\Delta\Gamma_\omega$  given by [30, 31, 23, 24]

$$\Delta\Gamma_\omega = 4\pi\rho_B \frac{m_n + m_\omega}{m_n m_\omega} \Im f_{\omega N}(0), \quad (1)$$

where  $m_N$  and  $m_\omega$  are the free nucleon and  $\omega$ -meson masses, respectively, while  $\rho_B$  is the baryon density. At the same time the  $\omega$ -meson mass shift  $\Delta m_\omega$  in nuclear

matter is given by [30,31,26]

$$\Delta m_\omega = -2\pi \rho_B \frac{m_n + m_\omega}{m_n m_\omega} \Re f_{\omega N}(0). \quad (2)$$

Here we propose phenomenological method to evaluate the forward  $\omega N$  scattering amplitude by coherent  $\omega$ -meson photoproduction off nuclei and to reconstruct the momentum dependence of the  $\omega$ -meson mass and width in nuclear matter. Our paper is organized as follows. In Sect. 2 we provide the formalism of the  $\omega$ -meson coherent photoproduction from nuclei. The analysis of available data as well as an estimation of the incoherent background are given in Sect. 3. In Sect. 4 we evaluate the forward scattering amplitude and compare our results with the predictions from available sources. The section ends with summary of our results.

## 2 Coherent $\omega$ photoproduction

The total cross section of  $\omega$ -meson photoproduction from nuclei,  $\gamma + A \rightarrow \omega + X$  is given by the sum of the coherent and incoherent processes. The differential cross section  $d\sigma_{\gamma A}^{coh}/dt$  for the coherent  $\omega$ -meson photoproduction from nuclei can be written in the eikonal form as [32,33,34,35,36,37]

$$\frac{d\sigma_{\gamma A}^{coh}}{dt} = \left| 2\pi f_{\gamma N}^{dif}(0) \int_0^\infty db J_0(k_t b) b \times \int_{-\infty}^\infty dz \rho(b, z) \exp[ik_l z + i\chi_\omega(b)] \right|^2, \quad (3)$$

where an integration is performed over the impact parameter  $b$  and  $z$  coordinate along the direction of the incident photon,  $\rho(r = \sqrt{b^2 + z^2})$  is the nuclear density function normalized to the total nucleon number  $A$ , while  $k_l$ ,  $k_t$  are the longitudinal and transverse component of the momentum transferred to the nucleus, respectively, given by

$$k_l = k_\omega - \sqrt{k_\omega^2 - m_\omega^2}, \quad k_t = 2k_\omega \sin(\theta/2), \quad (4)$$

with  $k_\omega$  is the total momentum,  $m_\omega$  is the pole mass of the  $\omega$ -meson and  $t$  is the squared four momentum transferred from the photon to  $\omega$ -meson. In (3)  $J_0$  is the zeroth order Bessel function and  $\chi_\omega$  is the nuclear phase shift related to  $\omega$ -meson distortion in nucleus. Within the  $t\rho$ -approximation this phase shift can be approximated by

$$\chi_\omega(b) = \frac{2\pi f_{\omega N}(0)}{k_\omega} \int_z^\infty \rho(b, y) dy, \quad (5)$$

where  $f_{\omega N}(0)$  is complex amplitude for the forward  $\omega N$  elastic scattering. The imaginary part of  $f_{\omega N}(0)$  is related by an optical theorem to the total cross section  $\sigma_{\omega N}$  of the  $\omega N$  interaction as

$$\Im f_{\omega N}(0) = \frac{k_\omega}{4\pi} \sigma_{\omega N}. \quad (6)$$

Now we introduce the ratio of the real to imaginary part of the forward scattering amplitude  $\alpha_\omega$  defined as

$$\alpha_\omega = \frac{\Re f_{\omega N}(0)}{\Im f_{\omega N}(0)} \quad (7)$$

and finally express the phase shift  $\chi_\omega$  as

$$\chi_\omega = \frac{\sigma_{\omega N}(i + \alpha_\omega)}{2} \int_z^\infty \rho(b, y) dy. \quad (8)$$

The quantity  $f_{\gamma N}^{dif}(0)$  in (3) is the forward diffractive  $\omega$ -meson photoproduction amplitude for a single nucleon related to the diffractive cross section  $d\sigma_{\gamma N}^{dif}/dt$  at  $t=0$  as

$$\frac{d\sigma_{\gamma N}^{dif}}{dt} \Big|_{t=0} = |f_{\gamma N}^{dif}(0)|^2, \quad (9)$$

ant can be expressed in a vector dominance model VDM in terms of the forward  $\omega N$  scattering amplitude  $f_{\omega N}(0)$ .

The total invariant amplitude  $\mathcal{M}_{\gamma\omega}$  for the reaction  $\gamma + N \rightarrow \omega + N$  is given by a VDM as

$$\mathcal{M}_{\gamma\omega} = \left[ \sum_{V=\rho,\phi,J/\Psi,\dots} \frac{\sqrt{\pi\alpha}}{\gamma_V} \mathcal{M}_{V\omega} \right] + \frac{\sqrt{\pi\alpha}}{\gamma_\omega} \mathcal{M}_{\omega\omega}, \quad (10)$$

where the summation is performed over the available vector meson states  $V$ . The quantity  $\alpha$  represents the fine structure constant,  $\gamma_V$  denotes the photon coupling to the vector meson state and  $\mathcal{M}_{V\omega}$  is the amplitude for the transition  $V + N \rightarrow \omega + N$  on a nucleon. Moreover, in (10)  $\gamma_\omega = 8.24 \pm 0.24$  is the photon- $\omega$  coupling constant evaluated [38] from the leptonic decays of the  $\omega$ -meson, and  $\mathcal{M}_{\omega\omega}$  is an invariant amplitude for the elastic scattering  $\omega + N \rightarrow \omega + N$ .

In principle, (10) might also contain the sum given by a non-diagonal transition of non-vector meson states to the  $\omega$ -meson as well as coupling of these possible intermediate continuum states to the photon. However, only the second term of (10) provides diffractive  $\omega$ -meson photoproduction on a nucleon and enters (3).

The differential cross section  $\gamma + N \rightarrow \omega + N$  is given by an invariant amplitude  $\mathcal{M}$  as

$$\frac{d\sigma_{\gamma N}}{dt} = \frac{|\mathcal{M}_{\gamma\omega}|^2}{64\pi s q_\gamma^2}, \quad (11)$$

where  $s$  is the squared invariant collision energy and  $q_\gamma$  is photon momentum in the center of mass system. Now, the forward diffractive  $\omega$ -meson photoproduction cross section on a single nucleon,  $d\sigma_{\gamma N}/dt$  at  $t=0$  can be expressed in terms of the  $\omega N$  forward scattering invariant amplitude  $\mathcal{M}_{\omega\omega}(0)$  as

$$\frac{d\sigma_{\gamma N}^{dif}}{dt} \Big|_{t=0} = \frac{1}{64s q_\gamma^2} \frac{\alpha}{\gamma_\omega^2} |\mathcal{M}_{\omega\omega}(0)|^2. \quad (12)$$

Furthermore, the scattering amplitude  $f_{\omega N}$  of (6) is related to the invariant scattering amplitude  $\mathcal{M}_{\omega\omega}$  as

$$f_{\omega N} = \frac{1}{8\pi\sqrt{s}} \frac{k_\omega}{q_\omega} \mathcal{M}_{\omega\omega}, \quad (13)$$

where  $k_\omega$  and  $q_\omega$  are the  $\omega$ -meson momenta in the laboratory and the  $\omega N$  center of mass system, respectively.

Finally, substituting (6) and (13) into (12) the differential cross section for the forward  $\omega$  meson photoproduction on a nucleon is given by

$$\left. \frac{d\sigma_{\gamma N}^{dif}}{dt} \right|_{t=0} = \frac{\alpha}{16\gamma_\omega^2} \frac{q_\omega^2}{q_\gamma^2} (1 + \alpha_\omega^2) \sigma_{\omega N}^2. \quad (14)$$

The differential cross section  $d\sigma_{\gamma A}^{coh}/dt$  for the coherent  $\omega$ -meson photoproduction from nuclei can then be written as

$$\begin{aligned} \frac{d\sigma_{\gamma A}^{coh}}{dt} = & \frac{\pi \alpha \sigma_{\omega N}^2 q_\omega^2}{4\gamma_\omega^2 q_\gamma^2} \left| (i + \alpha_\omega) \int_0^\infty db J_0(k_t b) b \int_{-\infty}^\infty dz \rho(b, z) \right. \\ & \left. \times \exp[ik_t z] \exp \left[ \frac{\sigma_{\omega N} (i\alpha_\omega - 1)}{2} \int_z^\infty \rho(b, y) dy \right] \right|^2. \quad (15) \end{aligned}$$

The parameters  $\alpha_\omega$  and  $\sigma_{\omega N}$  can be extracted from experimental data on coherent  $\omega$ -meson photoproduction from nuclei and through (6) and (7) should be converted to the real and imaginary part of the forward  $\omega N$  scattering amplitude. Furthermore, the coherent photoproduction can be measured at various photon beam momenta, thus providing the evaluation of the momentum dependence of the complex forward scattering amplitude  $f_{\omega N}(0)$ . In this way the momentum dependent potential of the  $\omega$ -meson in nuclear matter can be reconstructed

Eq.(15) illustrates that the absolute value of the  $\omega$ -meson coherent photoproduction differential cross section is very sensitive to the size of the total  $\omega N$  cross section,  $\sigma_{\omega N}$ , and thus to the imaginary part of the forward scattering amplitude  $\Im f_{\omega N}(0)$ . Therefore  $\Im f_{\omega N}(0)$  can be uniquely fixed by measuring the coherent  $\omega$ -meson photoproduction from nuclei.

To investigate the sensitivity of the coherent  $\omega$ -meson photoproduction on the real part of the forward scattering amplitude we calculate the coherent  $\omega$ -meson photoproduction cross section from  $Cu$  nuclei at a photon beam energy of  $E_\gamma=6.8$  GeV. In the calculations we use the nuclear density function  $\rho(r)$  given by a Wood-Saxon distribution as

$$\rho(r) = \frac{\rho_0}{1 + \exp[(r - R)/d]}, \quad (16)$$

with the nuclear radius being parameterized as

$$R = 1.28A^{1/3} - 0.76 + 0.8A^{-1/3} \text{ fm}, \quad (17)$$

and the diffusion parameter given by  $d=\sqrt{3}/3$  fm. Furthermore, for the moment we fix  $\sigma_{\omega N}$  at 35 mb, as will be motivated later.

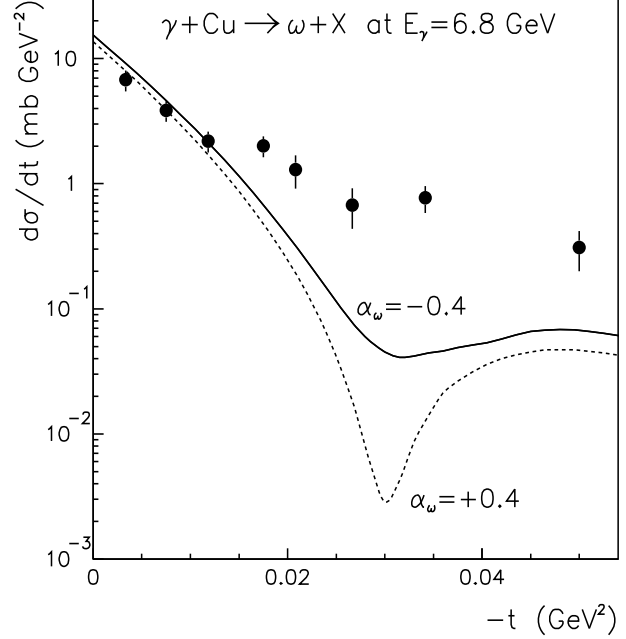


**Fig. 1.** The differential cross section for  $\omega$ -meson photoproduction from  $Cu$  target at photon energy  $E_\gamma=6.8$  GeV as a function of the squared four momentum transfer  $t$ . The lines show the calculations for the coherent  $\omega$ -meson photoproduction by Eq.15 with  $\sigma_{\omega N}=46$  mb and the ratio of the real to imaginary part of the  $\omega N$  forward scattering amplitude  $\alpha_\omega=0.4$  (dashed) and  $\alpha_\omega=-0.4$  (solid). The solid circles show the data [39] for the  $\omega$ -meson photoproduction where the contributions from both coherent and incoherent processes were not separated experimentally.

Fig.1 shows  $d\sigma_{\gamma A}^{coh}/dt$  calculated by (15) as a function of the square of four momentum transfer  $t$ . The solid line indicates the result calculated with the ratio of the real to imaginary part of the  $f_{\omega N}(0)$  taken as  $\alpha_\omega=-0.4$ , while the dashed line is the result for  $\alpha_\omega=0.4$ . It is clear that the ratio  $\alpha_\omega$  can be fixed only at the vicinity of the diffractive minima. Moreover, at the diffractive minima the calculated coherent  $\omega$ -meson photoproduction cross section indicates a substantial dependence on both, the absolute value and the sign of the ratio  $\alpha_\omega$ .

Furthermore, Fig.2 shows the differential cross section for the coherent photoproduction of  $\omega$ -mesons from a  $Cu$  target calculated around the diffractive minima at  $t= -0.03$  GeV<sup>2</sup> as a function of ratio  $\alpha_\omega$ . We found that around the diffractive minima the  $d\sigma_{\gamma Cu}^{coh}/dt$  is very sensitive to the  $\alpha_\omega$  and therefore, the real part of the forward scattering amplitude  $\Re f_{\omega N}(0)$  can be directly measured by coherent  $\omega$ -meson photoproduction. It is worthwhile to notice that this method allows a determination of the sign of  $\Re f_{\omega N}(0)$ .

The solid circles in Fig.1 show experimental results for  $\omega$ -meson photoproduction at an average photon energy  $E_\gamma=6.8$  GeV obtained by Behrend et al. [39] at the Cornell electron synchrotron. The produced  $\omega$ -mesons were detected through the  $\omega \rightarrow \pi^+ \pi^- \pi^0$  decay mode, thus the measurements [39] provide the data on inclusive  $\omega$ -meson

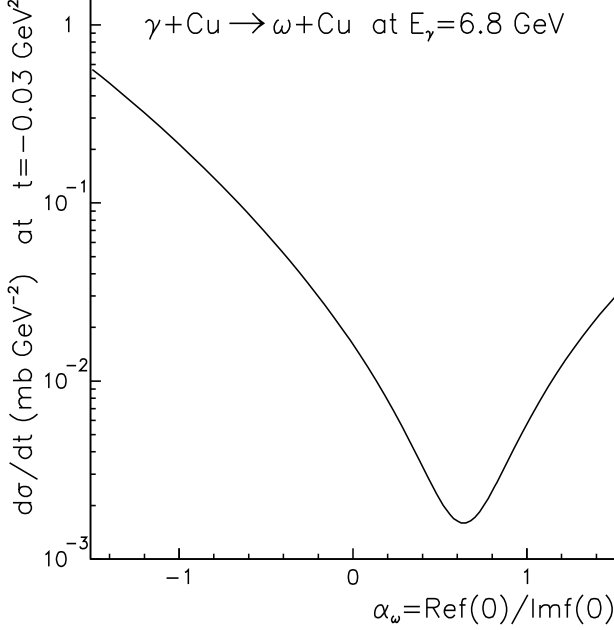


**Fig. 2.** The differential cross section for the coherent  $\omega$ -meson photoproduction from  $Cu$  target at photon energy  $E_\gamma=6.8$  GeV calculated around diffractive minima at  $t=-0.03$  GeV<sup>2</sup> as a function of the ratio  $\alpha$ .

photoproduction. The contributions from coherent and incoherent  $\omega$ -mesons photoproduction were not separated experimentally [39].

The experimental results on  $t$ -distribution shown by Fig.1 indicate a forward peak typical for the coherent  $\omega$ -meson photoproduction. The photoproduction at large  $|t|$  is dominated by incoherent production mechanism. Fig.1 illustrates that our calculations based on (15) reasonably reproduce the experimental results [39] at small  $|t|$  and manifest the dominance of the coherent photoproduction at  $t \geq -0.01$  GeV<sup>2</sup>. The data [39] can be used only for the evaluation of  $\sigma_{\omega N}$ , or imaginary part of the forward  $\omega N$  scattering amplitude.

### 3 Data analysis

As it was shown in Fig. 1 the comparison between our calculations and the experimental results requires an estimate of the contribution from the incoherent  $\omega$ -meson photoproduction. Moreover, the evaluation of the incoherent background is important for a determination of the experimental efficiency necessary for the separation of the coherent and incoherent  $\omega$ -meson photoproduction, especially near the diffractive minima, where the coherent cross section is sensitive to the real part of the  $\Re f_{\omega N}(0)$ .

Actually, the results shown in Fig. 1 indicate that for  $Cu$  targets and a photon energy of  $E_\gamma=6.8$  GeV the contribution from incoherent  $\omega$ -meson photoproduction around  $t \simeq -0.03$  GeV<sup>2</sup> may exceed the coherent one by two or three orders of magnitude. Whether this large difference

holds for other nuclear targets and photon energies requires an additional calculation of the incoherent  $\omega$ -meson photoproduction.

Taking into account only the leading term in  $t$  given by  $\omega$ -meson photoproduction and the absorption in the nucleus the differential cross section  $d\sigma_{\gamma A}^{inc}/dt$  for incoherent  $\omega$ -meson photoproduction is given by [34]

$$\frac{d\sigma_{\gamma A}^{inc}}{dt} = \frac{d\sigma_{\gamma N}^{tot}}{dt} \Big|_{t=0} \exp(at) \frac{2\pi}{\sigma_{\omega N}} \int_0^\infty b db \times (1 - \exp \left[ -\sigma_{\omega N} \int_{-\infty}^\infty \rho(b, y) dy \right]), \quad (18)$$

where  $a$  is the slope of  $t$ -distribution from the elementary reaction  $\gamma+N \rightarrow \omega+N$ . Furthermore, the elementary forward  $\omega$ -meson photoproduction cross section  $d\sigma_{\gamma N}^{tot}/dt$  at  $t=0$  now should account not only for the diffractive process due to the  $\omega+N \rightarrow \omega+N$  transition as is given by Eq.14, but also for the total  $\gamma N \rightarrow \omega N$  amplitude of (10).

However, as will be shown later, at high energies (14) accounts for the substantial part of a total forward  $\gamma+N \rightarrow \omega+N$  cross section. On the other hand,  $d\sigma_{\gamma N}^{tot}/dt$  at  $t=0$  as well as slope  $a$  can be evaluated from experimental data [40].

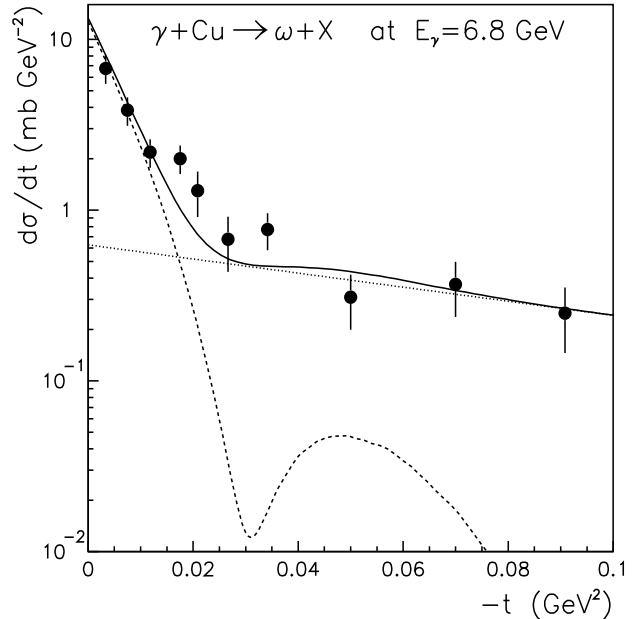


**Fig. 3.** The differential cross section for  $\omega$ -meson photoproduction from  $Cu$  nucleus at photon energy  $E_\gamma=6.8$  GeV as function of the squared four momentum transfer  $t$ . The solid circles show the data from Ref. [39]. The dashed line indicates the calculations for the coherent  $\omega$ -meson photoproduction by Eq.15, while the dotted line is the incoherent  $\omega$  photoproduction cross section given by Eq.18. The solid line shows their sum. The calculations were performed with  $\sigma_{\omega N}=46$  mb, the ratio  $\alpha_\omega=0$  and slope  $a=9.5$  GeV<sup>-2</sup>.

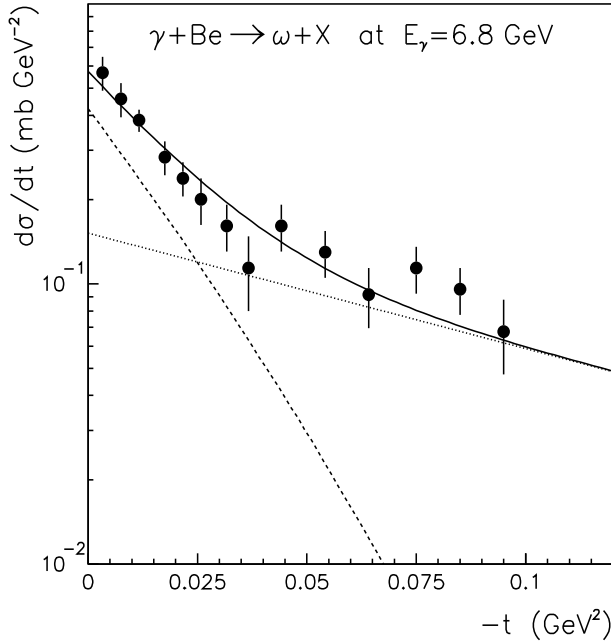


**Fig. 4.** The differential cross section for  $\gamma Be \rightarrow \omega X$  reaction at  $E_\gamma = 6.8$  GeV as a function of the squared four momentum transfer  $t$ . The solid circles show the data from Ref. [39]. The dashed line indicates the calculations for the coherent  $\omega$ -meson photoproduction by Eq.15, the dotted line is incoherent  $\omega$  photoproduction cross section given by Eq.18, while the solid line shows their sum. The calculations were performed with  $\sigma_{\omega N} = 46$  mb, the ratio  $\alpha_\omega = 0$  and slope  $a = 9.5$  GeV $^{-2}$ .

Moreover, higher order corrections to (18) due to the single elastic scattering after the  $\omega$ -photoproduction on a target nucleon are proportional to the powers of  $\exp(at)$  and might be important only at large  $|t|$ . However, this is beyond the region of our interest. We also do not consider photon shadowing, which might play certain role in the incoherent  $\omega$ -meson photoproduction.

The differential cross section for  $\gamma + Cu \rightarrow \omega + X$  reaction at  $E_\gamma = 6.8$  GeV. is shown in Fig. 3. Solid circles represent experimental results from Ref. [39]. The lines show the calculations performed with  $\sigma_{\omega N} = 46$  mb, the ratio  $\alpha_\omega = 0$  and a slope  $a = 9.5$  GeV $^{-2}$  [40]. Here we also take  $d\sigma_{\gamma N}^{tot}/dt$  at  $t=0$  as given by (14). The dashed line in Fig. 3 shows our result for the differential cross section for coherent  $\omega$ -meson photoproduction calculated by (15). The dotted line indicates the result for the incoherent  $\omega$ -meson photoproduction as calculated by (18). The solid line is the sum of coherent and incoherent processes and reasonably describes the data [39].

Fig. 4 shows the differential cross section for  $\omega$ -meson photoproduction from  $Be$  at a photon energy  $E_\gamma = 6.8$  GeV. Again, the experimental results are taken from Ref. [39] and the lines show the calculations with  $\sigma_{\omega N} = 46$  mb,  $\alpha_\omega = 0$  and  $a = 9.5$  GeV $^{-2}$  [40]. The results for coherent and incoherent  $\omega$ -meson photoproduction are shown by the dashed and dotted lines, respectively. The solid line indicates their sum and describes the data reasonably well.

Note that the position of the diffractive minima for light nuclei lies at substantially larger  $|t|$  [41].

In the calculations for  $Be$  we use the density function given by [42]

$$\rho(r) = \frac{1}{(R\sqrt{\pi})^3} \left[ 4 + \frac{2(A-4)r^2}{3R^2} \right] \exp \left[ -\frac{r^2}{R^2} \right], \quad (19)$$

where  $R = 1.58$  fm.

The  $\omega$ -meson photoproduction from nuclei at average photon energies  $E_\gamma = 8.2$  GeV was studied experimentally by Aramson et al. [43] with results compatible to their previous measurements given at  $E_\gamma = 6.8$  GeV in Ref. [39].

In addition, the  $\omega$ -meson nuclear photoproduction at average photon energies  $E_\gamma = 5.7$  GeV was measured at DESY [44] by detecting the  $\omega \rightarrow \pi^0 \gamma$  decay. The coherent and incoherent processes were not separated and the data were published without absolute normalization.

Fig.5 shows the differential cross section for  $\omega$ -meson photoproduction from  $C$  and  $Al$  targets at photon beam energy  $E_\gamma = 5.7$  GeV. The DESY experimental results are taken from Ref. [44] and normalized by our calculations. The solid lines show the sum of the coherent and incoherent photoproduction cross sections. The dotted lines show the calculations for incoherent  $\omega$ -meson photopro-

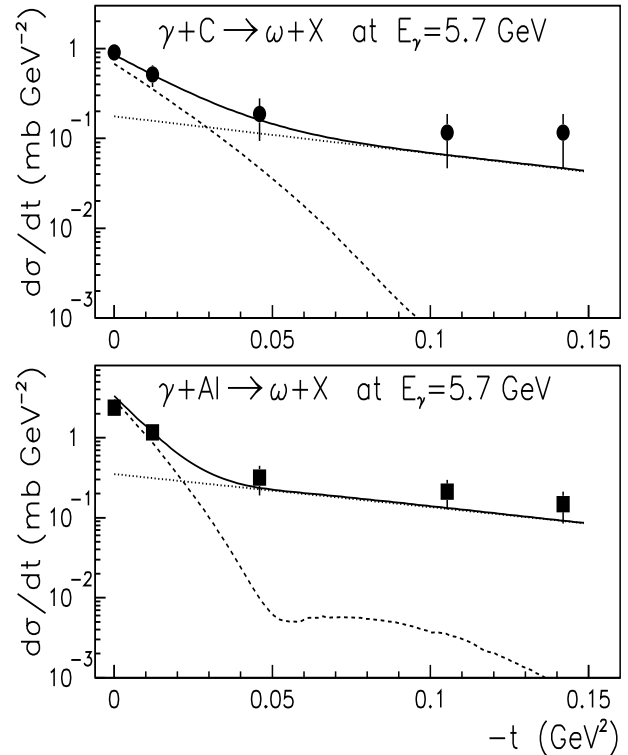


**Fig. 5.** The differential cross section for  $\omega$ -meson photoproduction from  $C$  and  $Al$  at  $E_\gamma = 5.7$  GeV as a function of the squared four momentum transfer  $t$ . The data were taken from Ref. [44]. The lines show our results for the coherent (dashed), incoherent (dotted) and the sum (solid) of coherent and incoherent photoproduction given by Eqs.15,18 and calculated with  $\sigma_{\omega N} = 46$  mb, ratio  $\alpha_\omega = 0$  and slope  $a = 9.5$  GeV $^{-2}$ .

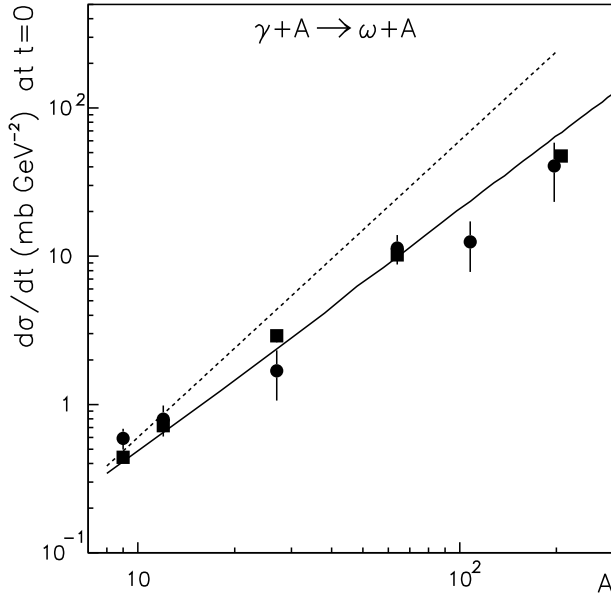


**Fig. 6.** The differential cross section for  $\omega$ -meson photoproduction at  $t=0$  as a function of target mass number  $A$ . The circles show the data [45] for photon beam energy  $E_\gamma=3.9$  GeV, while the squares show the results [46] measured at  $E_\gamma=6.8$  GeV. The solid line shows our calculations with  $\sigma_{\omega N}=37$  mb and  $\alpha_\omega=0$ . The dashed line indicates the  $A^2$ -dependence obtained with  $\sigma_{\omega N}=0$ .

duction, which is dominant at large  $|t|$ . The contribution from coherent  $\omega$ -meson photoproduction is given by the dashed lines. The calculations were performed using (15) and (18) with parameters  $\sigma_{\omega N}=46$  mb,  $\alpha_\omega=0$  and  $a=9.5$  GeV $^{-2}$  [40].

The data [44] are quite reasonably reproduced by the calculations. However, they are insensitive to the ratio  $\alpha$ . Our choice of  $\alpha_\omega=0$  for the comparison between the calculations and the data [39,44] is indeed arbitrary. We conclude that the ratio  $\alpha$  as well as the real part of the forward  $\omega N$  scattering amplitude  $\Re f_{\omega N}(0)$  can not be constrained by the available data [39,43,44], since these measurements did not isolate the coherent photoproduction.

The total coherent and incoherent  $\omega$ -meson photoproduction cross sections from complex nuclei at  $E_\gamma=3.9$  GeV were measured by Brodbeck et al. [45] and extrapolated to  $t=0$ . Experimental results for  $\omega$ -meson photoproduction from nuclei at  $E_\gamma=6.8$  GeV and at  $t=0$  were also reported by Behrend et al. [46].

Fig.6 shows results for  $\omega$ -meson photoproduction cross section at  $t=0$  as a function of the target mass number. The solid circles indicate data [45] collected at  $E_\gamma=3.9$  GeV, while the squares show the results [46] measured at photon energy  $E_\gamma=6.8$  GeV. The data do not show any dependence on the photon beam energy.

The solid line in Fig.6 indicates our calculations with  $\sigma_{\omega N}=37$  mb and ratio  $\alpha_\omega=0$ . We note that our results do not depend on the ratio  $\alpha$ . The dashed line in Fig. 6 shows the  $A^2$ -dependence which is given by (15) assuming that

$\sigma_{\omega N}=0$  and neglecting the  $k_l$ -dependence. The dashed line is arbitrary normalized at  $A=Be$ .

Moreover, the difference between the solid and dashed lines in the Fig. 6 is due to the finite value of  $\sigma_{\omega N}$ . Therefore, the data [45,46,46] on forward  $\omega$ -meson photoproduction provide a reasonable evaluation of the imaginary part of the  $\omega N$  forward scattering amplitude  $\Im f_{\omega N}(0)$ .

## 4 Evaluation of the forward scattering amplitude

The comparison between our calculations and experimental results [39,43,44,45] allows us to extract the imaginary part of the forward  $\omega N$  scattering. Finally the data on  $\omega$ -meson photoproduction from nuclei were fitted in order to evaluate  $\sigma_{\omega N}$ . Although we found that the available data are absolutely insensitive to the ratio  $\alpha_\omega$ , we allow its variation by a minimization procedure [47].

The results of the minimization are shown in the Table. 1. None of the data sets allows to extract a specific value for the ratio  $\alpha_\omega$ . Some of the experimental results allow an extraction of  $\sigma_{\omega N}$  with sufficiently large uncertainty.

However, we should clarify, that experimental results are insensitive to the ratio  $\alpha_\omega$  in case it is less than one. As is shown by (15) the large values of  $\alpha_\omega$  should immediately effect our results. Roughly, a large ratio  $\alpha_\omega$  should cause a decrease of the total  $\omega N$  cross section  $\sigma_{\omega N}$ . The fitting procedure does not indicate such a tendency. Our analysis suggest that  $\alpha_\omega < 1$  or  $\Im f_{\omega N}(0) > \Re f_{\omega N}(0)$ .

Moreover, the  $\omega$ -meson photoproduction data on  $A$ -dependence at  $t=0$  shown in the Fig.6 show substantial sensitivity to  $\sigma_{\omega N}$ . Obviously, the situation might improve substantially when separate data for coherent photoproduction will be available.

**Table 1.** The total  $\omega N$  cross section  $\sigma_{\omega N}$  in mb and the ratio of the real to imaginary  $\omega N$  scattering amplitude  $\alpha_\omega$  evaluated from the data on  $\omega$ -meson photoproduction from nuclei at photon energy  $E_\gamma$  given in GeV. Also are shown the total  $\chi^2$ , number of experimental points  $nep$  and the legend and the reference to experimental results.

$E_\gamma$	$\sigma_{\omega N}$	$\alpha_\omega$	$\chi^2$	$nep$	legend	Ref.
3.9	$36.1 \pm 2.2$	$0.17 \pm 0.20$	10.2	6	$t=0$	[45]
6.8	$36.8 \pm 2.0$	$-0.01 \pm 0.03$	33.8	5	$t=0$	[46]
6.8	$45.9 \pm 1.3$	$0.2 \pm 0.1$	11.5	14	$Be$	[39]
6.8	$44.8 \pm 0.1$	$-0.11 \pm 0.02$	14.6	14	$Cu$	[39]
5.7	$48 \pm 4$	$0.15 \pm 0.18$	1.4	5	$C$	[44]
5.7	$44 \pm 2$	$0.05 \pm 0.02$	5.4	5	$Al$	[44]

Final results for  $\sigma_{\omega N}$  are converted by (6) to imaginary part of  $f_{\omega N}(0)$  and are shown by the solid circles in Fig.7 as a function of the total laboratory  $\omega$ -meson energy  $E_\omega$ . In the case, when the results for  $\sigma_{\omega N}$  are evaluated from different data sets but at the same photon energy,

we average them in calculating the imaginary part of the forward scattering amplitude.

Now our results can be compared with estimations given by (6) and (14) and available data on forward  $\omega$ -meson photoproduction on a free nucleon. The squares in Fig.7 show the  $\Im f_{\omega N}(0)$  obtained from the data [40] on  $\gamma+p \rightarrow \omega+p$  reaction cross section at  $t=0$  and neglecting the ratio  $\alpha_\omega$  in (14).

An arrow at Fig. 7 indicates the lower limit for the imaginary part of the  $\omega N$  scattering amplitude at threshold  $E_\omega=m_\omega$  given at the pole mass of  $\omega$ -meson by

$$\Im f_{\omega N}(0) = 0.164 \text{ fm}, \quad (20)$$

as recently evaluated [48] from  $\pi^-+p \rightarrow \omega+n$  measurements [49].

Moreover, within an additive quark model the forward  $\omega N$  scattering amplitude is given as the average of the forward  $\pi^-N$  and  $\pi^+N$  amplitudes [50,51,52]. Using the Donnachie and Landshoff results [53] for a Regge theory fit to the  $\pi N$  total cross section the complex forward  $\omega N$  scattering amplitude can be written as

$$f_{\omega N}(0) = \frac{k_\omega}{4\pi \hbar c} \left[ \left( 0.173 \left[ \frac{s}{s_0} \right]^\epsilon - 2.726 \left[ \frac{s}{s_0} \right]^{-\eta} \right) \right]$$

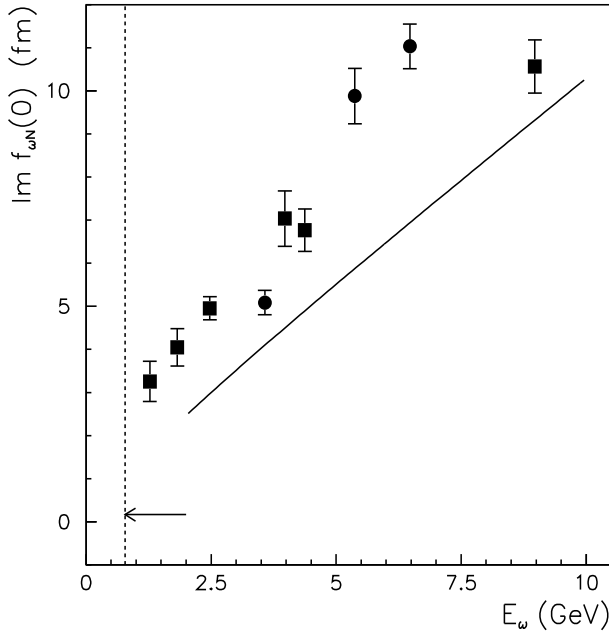


**Fig. 7.** The imaginary part of the forward  $\omega N$  scattering amplitude  $\Im f_{\omega N}(0)$  as a function of laboratory  $\omega$ -meson total energy  $E_\omega$ . The solid circles show our results extracted from  $\omega$ -meson photoproduction off nuclei. The squares show the result evaluated by (6) and (14) from the data [40] on forward  $\omega$ -meson photoproduction in  $\gamma+p \rightarrow \omega+p$  reaction. The dashed line shows the  $\omega N$  threshold given by  $\omega$ -meson pole mass. The arrow indicates the lower limit for  $\Im f_{\omega N}(0)$  at threshold obtained [48] from the  $\pi+N \rightarrow \omega+N$  data [49]. The solid line is the predictions from additive quark model and Regge theory given by (21).

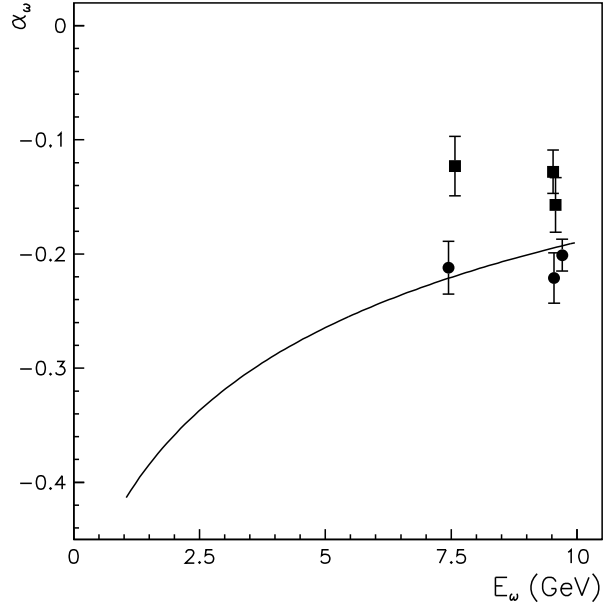


**Fig. 8.** The ratio  $\alpha_\omega$  of the real to imaginary part of the forward  $\omega N$  scattering amplitude as a function of total laboratory  $\omega$ -meson energy  $E_\omega$ . The solid circles show experimental results [54] for  $\pi^+p$  scattering taken at the same invariant collision energy  $\sqrt{s}$ , while the squares are that for  $\pi^-p$  scattering [54]. The solid line shows the predictions for  $\omega N$  scattering given by an additive quark model and Regge theory [52] and calculated by (21).

$$+i \left( 1.359 \left[ \frac{s}{s_0} \right]^\epsilon + 3.164 \left[ \frac{s}{s_0} \right]^{-\eta} \right) \text{ fm}, \quad (21)$$

where the  $\omega$ -meson momentum  $k_\omega$  and squared invariant collision energy  $s$  are given in GeV/c and  $s_0=1 \text{ GeV}^2$ . The effective powers  $\epsilon=0.08$  and  $\eta=0.45$  are given by the pomeron and  $\rho$ ,  $\omega$ ,  $f$ ,  $a$  exchanges, respectively. The solid line in Fig. 7 shows the prediction by additive quark model calculated by (21). We find that the prediction from the additive quark model and the Regge theory systematically underestimates other results.

Although we do not consider the results for ratio  $\alpha_\omega$  listed in the Table 1 at some confidence level, it seems worthwhile to discuss a possible estimate for the ratio of the real to imaginary part of the forward  $\omega N$  scattering amplitude. Moreover, as is illustrated by Fig.2 the magnitude of the coherent differential  $\omega$ -meson photoproduction cross section at diffractive minima substantially depends on the both sign and size of the  $\alpha_\omega$  and thus the estimate for this ratio may be useful for valuation of an experimental accuracy necessary for measurements around the diffractive minima.

Very rough estimates of the ratio  $\alpha_\omega$  may be given by an additive quark model through (21) and is shown in Fig.8 by the solid line as a function of total  $\omega$ -meson laboratory energy  $E_\omega$ . The solid circles in the Fig.8 show the experimental results [54] for the ratio of the real to imaginary part for the  $\pi^-p$  forward scattering amplitude

while the squares indicate the data for  $\pi^+p$  scattering. The  $\pi N$  data were taken at the same invariant collision energies  $\sqrt{s}$ .

Furthermore, the results from the coupled channel analysis [23] of the meson-nucleon scattering data predicts at the  $\omega N$  threshold

$$f_{\omega N} = -0.5 + i0.2 \text{ fm}, \quad (22)$$

providing the negative ratio  $\alpha_\omega = -2.5$ . Moreover, most recently within the same model approach [24] it was deduced that  $\Im f_{\omega N} = 0.013 \text{ fm}$ , while the real part  $\Re f_{\omega N}$  stands the same as in Eq.22 resulting finally in the ratio  $\alpha_\omega = -38.5$ .

At the same time, the calculations [25] based on an effective Lagrangian approach combined with chiral SU(3) dynamics predicts the forward  $\omega N$  scattering amplitude as

$$f_{\omega N} = 3.34 + i2.1 \text{ fm}, \quad (23)$$

with a positive defined ratio  $\alpha_\omega = 0.62$ . More recent results of the calculation [26] of the scattering amplitude is given as

$$f_{\omega N} = 1.6 + i0.3 \text{ fm}, \quad (24)$$

with positive and large ratio  $\alpha_\omega = 5.3$ .

Theoretical predictions available for  $\alpha_\omega$  differ substantially both in sign and the absolute value of the ratio. Obviously, the coherent  $\omega$ -meson photoproduction from nuclei can not directly resolve the existing discrepancies between available predictions for the forward  $\omega N$  scattering amplitude exactly at  $E_\omega = m_\omega$ . However the  $\gamma + A \rightarrow \omega + A$  reactions might be considered as a model independent measurements of  $f_{\omega N}$  at final  $\omega$ -meson momenta as well as provide an orientation for analytical continuation of the forward scattering amplitude close to the threshold [55, 56, 57].

It is important to note that both, the coherent and incoherent cross sections for forward  $\omega$ -meson photoproduction from nuclei will be influenced when large values of  $\alpha > 1$  are used.

## 5 Conclusions

The coherent  $\omega$ -meson photoproduction from nuclei is studied as a possible phenomenological method to evaluate the complex forward  $\omega N$  scattering amplitude at finite  $\omega$ -meson momenta.

We found that the real part of the forward scattering amplitude  $\Re f_{\omega N}(0)$  can be only fixed by the data on coherent  $\omega$ -meson photoproduction around the diffractive minima. At the same time, the imaginary part of the forward scattering amplitude  $\Im f_{\omega N}(0)$  can be well evaluated by an absolute value of the cross section at small  $|t|$ , where the contribution from incoherent processes is relatively small. Moreover, the sign and the magnitude of the ratio  $\alpha_\omega$  of the real to imaginary part of the forward  $\omega N$  scattering amplitude can be identified by the magnitude of the coherent photoproduction cross section at diffractive minima.

We analyze available experimental data [39, 43, 44, 45, 46] on  $\omega$ -meson photoproduction from nuclei. Unfortunately the contributions from coherent and incoherent processes are not separated experimentally. We find reasonable agreement between the data [39, 43, 44, 45, 46] and our calculations including both, coherent and incoherent  $\omega$ -meson photoproduction. By fitting the experimental results we evaluate the imaginary part of the forward  $\omega N$  scattering amplitude. Within our approach we do not vary the  $\omega$ -photon coupling constant, but fix it by the dileptonic decay. We find that data, which are not separated into coherent and incoherent production, can not provide reliable results for the real part of the scattering amplitude  $\Re f_{\omega N}(0)$ .

Finally, our results for  $\Im f_{\omega N}(0)$  are compared with predictions given by a vector dominance model relation between the forward  $\gamma + N \rightarrow \omega + N$  reaction cross section and imaginary part of the forward  $\omega N$  scattering amplitude. The experimental data [40] for forward  $\omega$ -meson photoproduction from the proton provide an  $\Im f_{\omega N}(0)$  that agrees reasonably well with our estimates.

Furthermore, the predictions by an additive quark model together with a Regge model fit to the data for hadronic cross sections systematically underestimate our results for  $\Im f_{\omega N}(0)$  as well as that extracted from the  $\gamma + p \rightarrow \omega + p$  reaction. This discrepancy might indeed indicate that, while experimental results on exclusive  $\rho$ ,  $\phi$  and  $J/\Psi$  photoproduction excellently confirm [52, 53, 57] the Regge theory, the  $\omega$ -meson photoproduction could be considered as an exception. It is important that  $\Im f_{\omega N}(0)$  is evaluated precisely from available data on the  $A$ -dependence of  $\omega$ -meson photoproduction at  $t=0$ .

We also discuss the current status of the predictions for the real part of the  $\omega N$  scattering amplitude and detect a strong disagreement between the results from different models.

This work was performed in part under the auspices of the U. S. Department of Energy under contract No. DE-FG02-93ER40756 with the Ohio University.

## References

1. G. Agakichiev et al., Phys. Rev. Lett. **75**, (1995) 1272.
2. G. Agakichiev et al., Phys. Lett. B **422**, (1998) 405.
3. G. Agakichiev et al., Nucl. Phys. A **661**, (1999) 23.
4. M. Masera et al., Nucl. Phys. A **590**, (1992) 93.
5. G.E. Brown and M. Rho, Phys. Rev. Lett. **66**, (1991) 2720.
6. G.Q. Li, C.M. Ko and G.E. Brown, Phys. Rev. Lett. **75**, (1995) 4007.
7. R. Rapp, G. Chanfray and J. Wambach, Nucl. Phys. A **617**, (1997) 472.
8. W. Cassing and E. Bratkovskay, Phys. Rept. **308**, (1999) 65.
9. J. Friese et al. Prog. Part. Nucl. Phys. **42**, (1999) 235.
10. J. Friese et al., Nucl. Phys. A **654**, 1017 (1999).
11. J. Stroth et al., Adv. Nucl. Dyn. **5**, (1999) 311.
12. D.P. Morrison et al. Nucl. Phys. A **638**, (1998) 565.



13. W.A. Zajc et al., Proc. of 15th Int. Conf. on Ultrarelativistic Nucleus-Nucleus Collisions, QM2001, Stony Brook, New York (2001).
14. J.G. Messchendorp et al., Eur. Phys. J. A **11**, (2001) 95.
15. A. Sibirtsev, V. Hejny, H. Ströher and W. Cassing, Phys. Lett. B **483**, (2000) 405.
16. V. Metag, Acta Phys. Pol. B **31**, (2000) 197.
17. E.L. Bratkovskaya, W. Cassing and U. Mosel, Nucl. Phys. A **686**, (2001) 568.
18. Effenberger, E.L. Bratkovskaya and U. Mosel, Phys. Rev. C **60**, (1999) 044614.
19. A.R. Gabler et al., Nucl. Instr. Meth. A **346**, (1994) 168.
20. E. Aker et al, Nucl. Instr. Meth. A **321**, (1992) 69.
21. E. Golubeva et al., Eur. Phys. J. A **11**, (2001) 237.
22. K. Tsushima, D.H. Lu, A.W. Thomas and K. Saito, Phys. Lett. B **443**, (1998) 26.
23. B. Friman, M. Lutz and G. Wolf, Proceedings of 28-th Int. Workshop on Gross Properties of Nuclei and Nuclear Excitation: Hadrons in Dense Matter, Hirschegg, Austria, (2000) 161.
24. B. Friman, Acta Phys. Pol. B **29**, (1998) 3195.
25. F. Klingl, N. Kaiser and W. Weise, Nucl. Phys. A **624**, (1997) 527.
26. F. Klingl, T. Waas and W. Weise, Nucl. Phys. A **650**, (1999) 299.
27. K. Saito, K. Tsushima, D.H. Lu and A.W. Thomas, Phys. Rev., C **59**, (1999) 1203.
28. G.I. Lykasov, W. Cassing, A. Sibirtsev and M.V. Rzyanin, Eur. Phys. J. A **6**, (1999) 71.
29. K. Ozawa et al., Phys. Rev. Lett. **86**, (2001) 5019.
30. W. Lenz, Z. Phys. **56**, (1929) 778.
31. C.D. Dover, J. Hüfner and R.H. Lemmer, Ann Phys. **66**, (1971) 248.
32. M. Ross and L. Stodolsky, Phys. Rev. **149**, (1966) 1172.
33. S.D. Drell and J.S. Trefil, Phys. Rev. Lett. **16**, (1966) 552.
34. K.S. Kölbig and B. Margolis, Nucl. Phys. B **6**, (1968) 85.
35. T.H. Bauer, R.D. Spital and D.R. Yennie, Rev. Mod. Phys. **50**, (1978) 261.
36. J.S. Trefil, Phys. Ref. **180**, (1969) 1379.
37. J.S. Trefil, Nucl. Phys. B **11**, 330 (1969).
38. A. Sibirtsev and W. Cassing, Eur. Phys. J. A **7**, (1998) 407.
39. H.-J. Behrend et al., Phys. Rev. Lett. **24**, (1970) 1246.
40. Landol-Börnstein, New Series **I/8**, Springer-Verlag.
41. A. Sibirtsev and W. Cassing, Phys. Rev. C **61**, (2000) 057601.
42. O.D. Dalkarov and V.A. Karmanov, Nucl. Phys. A **445**, (1985) 579.
43. J. Abramson et al., Phys. Rev. Lett. **36**, (1976) 1428.
44. P.L. Braccini et al., Nucl. Phys. B **24**, (1970) 173.
45. T.J. Brodbeck et al., Nucl. Phys. B **136**, (1978) 95.
46. H.-J. Behrend et al., Phys. Rev. Lett. **27**, (1971) 65.
47. F. James and M. Roos, Comp. Phys. Comm. **10**, (1975) 343.
48. C. Hanhart, A. Sibirtsev and J. Speth, sub. to Phys. Rev. C.
49. H. Karami et al. Nucl. Phys. B **154**, (1979) 503.
50. H.J. Lipkin, Phys. Rev. Lett. **16**, (1966) 1015.
51. K. Kajantie and J.S. Trefil, Phys. Lett. B **24**, (1967) 106.
52. A. Donnachie and P.V. Landshoff, Phys. Lett. B **348**, (1995) 213.
53. A. Donnachie and P.V. Landshoff, Phys. Lett. B **296**, (1992) 227.
54. K.J. Foley et al., Phys. Rev. **181**, (1969) 1775.
55. V.L. Eletsky and B.L. Ioffe, Phys. Rev. Lett. **78**, (1997) 1010.
56. L.A. Kondratyuk et al., Phys. Rev. C **58**, (1998) 1078.
57. A. Sibirtsev, K. Tsushima and A.W. Thomas, Phys. Rev. C **63**, (2001) 044906.